Particle transport in the scrape-off layer and its relationship to discharge density limit in Alcator C-Mod

B. LaBombard*, R.L. Boivin, M. Greenwald, J. Hughes, B. Lipschultz,

D. Mossessian, C.S. Pitcher, J.L. Terry, S.J. Zweben†, Alcator Group

Massachusetts Institute of Technology, Plasma Science and Fusion Center,

175 Albany St., Cambridge, MA 02139 USA

†*Princeton Plasma Physics Laboratory, Princeton, NJ 08543 USA*

Cross-field particle transport in the scrape-off layer (SOL) of Alcator C-Mod [Phys. Plasmas **1**, 1511 (1994)] can be characterized by an effective particle diffusivity (D_{eff}) that increases markedly with distance from the separatrix. As a consequence, recycling onto the main-chamber walls is large compared to plasma flows into the divertor volume. The SOL exhibits a two-layer structure: Steep gradients and moderate fluctuation levels are typically found in a ~5 mm region near the separatrix (near SOL) where parallel electron conduction typically dominates energy losses. Small gradients and larger fluctuation levels with longer correlation times are found outside this region (far SOL). D_{eff} in the near SOL increases strongly with local plasma collisionality normalized to the magnetic connection length. As the discharge density limit is approached, D_{eff} and associated fluctuation levels become large across the entire SOL and cross-field heat convection everywhere exceeds parallel conduction losses, impacting the power balance of the discharge.

PACS: 52.25.Fi, 52.25.Gj, 52.40.Hf, 52.55.Fa, 52.70.Ds, 52.70.Kz, 52.70.Nc

---

*Tel.: 1-617-253-6942, Fax: 1-617-253-0627: e-mail: labombard@psfc.mit.edu.

I. INTRODUCTION

Cross-field particle transport near the separatrix and in the scrape-off layer (SOL) directly influences the operation of a tokamak and needs to be understood in a way that can be scaled to reactor conditions. The effectiveness of the divertor in receiving plasma exhaust and controlling neutral pressures in the main-chamber volume critically depends on particle transport in the SOL. If cross-field plasma transport is sufficiently high, then plasma flows onto wall surfaces in the main-chamber volume will become large compared to plasma flows along field lines into the divertor volume. In Alcator C-Mod[1], this situation is routinely encountered[2,3] and is termed a 'main-chamber recycling' (MCR) regime. Impurity levels in the core plasma not only depend on the level of plasma-wall interaction in the main chamber but also depend on particle transport behavior near the separatrix. For example, high confinement mode plasmas (H-modes) which are free of edge localized modes (ELMs) typically end in a radiation-induced collapse caused by impurity accumulation. In contrast, enhanced D_α H-modes in Alcator C-Mod (EDA)[4] avoid impurity accumulation; a quasi-coherent edge fluctuation associated with EDA provides increased particle transport across the separatrix[5]. Finally, as discussed in this paper, there is reason to believe that cross-field particle transport at the separatrix and its dependence on discharge conditions plays a key role in setting the maximum edge density that can be achieved in gas-fueled discharges and impacting the discharge density limit.

In this paper, we examine the behavior of cross-field particle transport and resultant heat convection through the separatrix, across the SOL, and onto main-chamber surfaces for a number Alcator C-Mod discharges. The discharges and the diagnostic tools used for this work are discussed in section II. A technique of inferring effective cross-field particle diffusion coefficients (D_{eff}) from profile data described in Ref [3] is summarized in section III. This technique utilizes the observation that C-Mod operates predominantly in a MCR regime such that cross field plasma flux profiles can be inferred directly from ionization profiles. Section IV extends regression analysis results reported in Ref [3], correlating D_{eff} with local plasma conditions in discharges with

different plasma currents and magnetic fields. It is found that D_{eff} in a ~5 mm zone near the separatrix (near SOL) is well correlated with the local values of electron-ion mean free path normalized to the magnetic connection length, $D_{eff} \sim (\lambda_{ei}/L)^{-1.7}$. Section V describes plasma fluctuations and the behavior of fluctuations and heat convection as the discharge density limit is approached. Consistent with the finding that D_{eff} increases rapidly with distance from the separatrix, the amplitude and character of plasma fluctuations in the near and far SOL zones is markedly different. Near the density limit, cross-field heat convection clearly dominates over parallel conduction losses over the entire SOL and becomes an important component in the power balance of the discharge. Section VI draws connections between this work and transport/fluctuation observations made in other experiments. Section VII summarizes the principal findings.

II. EXPERIMENTAL ARRANGEMENT

All results reported in this paper were obtained in deuterium discharges with a diverted, lower single-null magnetic equilibrium, similar to that of Fig. 1. Only ohmically heated discharges are investigated in this paper since their moderate power densities enables the use of probe diagnostics to investigate the SOL. More detailed information on the first-wall geometry and the edge diagnostic set can be found in Ref. [3].

Referring to Fig. 1, the following surface areas can be defined based on line segments in the poloidal plane, revolved about the torus centerline: *Divertor throat* spans across the X-point region, from probe 8 on the outer divertor to probe 4 on the inner divertor. *Divertor target* includes segments that span from probe 1 to 8 on the outer and from probe 1 to 4 on the inner divertor. *Main-chamber surface* includes all surfaces above the *divertor throat. Divertor baffle* includes segments that span from probe 8 to 10 on the outer and from probe 4 to 6 on the inner divertor.

Primary limiter structures in the main chamber consist of a toroidally continuous inner-wall limiter, and principally two discrete outboard limiters spanning ~6 degrees toroidally and separated by ~180 degrees toroidally. Secondary limiter structures exist ~5 mm (mapped to midplane)

beyond the shadow of primary limiters at a number of toroidal locations. These are used to minimize plasma density at the surface of ICRF antennas which are in turn displaced another ~5 mm further into the SOL. Separatrix-to-limiter gaps for most of the data reported here were 18 to 20 mm (mapped to midplane), with inner and outer gaps similar. Density limit discharges (in section V) had a reduced outer gap of 12 mm. Scrape-off layer flux surfaces which miss the limiters terminate on the divertor target or baffle surfaces.

Mounted onto the side of one outboard limiter, 15 cm above the midplane (see Fig.1), is a cylindrical Langmuir probe which spans a 14 mm zone from the leading edge into the shadow of the limiter. The signal of this 'limiter shadow particle flux probe' (LSFP) corresponds to a spatial integral of local ion saturation current density across the local shadow of the limiter. Magnetic field lines which terminate on this probe extend only a short distance (L = 1.1 m) and terminate on an adjacent limiter structure. As a result, the ratio of ionization rate to plasma loss rate out the ends of the 'flux tube' intercepted by the probe, $n_0 \langle \sigma v \rangle_{ion} L / C_s$, is typically much less than one. [Here n_0 is the local neutral density (< ~5x10^{17} m^{-3}, estimated from midplane pressure measurements and neutral flux balance), $\langle \sigma v \rangle_{ion}$ is the ionization rate (~10^{-14} m^3 s^{-1}), and C_s is the local sound speed (~ 3x10^4 m s^{-1})]. Therefore, the ion current collected by the probe arises primarily from plasma diffusing across field lines into the local limiter shadow over a wide range of plasma conditions. Using simple geometry, the probe signal can be related to the cross-field ion flux arriving at the edge of the local limiter shadow. The edge of the local limiter shadow is located 4 to 5 mm (mapped to midplane) beyond a magnetic flux surface which is tangent to the outboard limiters. [See Fig.1: The outer-most flux surface shown is tangent to the outboard limiter. At the poloidal location of the LSFP, the edge of the outer limiter (and the LSFP) is located 4 to 5 mm beyond this flux surface.]

Absolutely calibrated D_α brightnesses from radial chords which span a vertical extent of 0.1 m about the plasma center are recorded by a photodiode array. For the present studies, the chords

are located 30 cm toroidally from an outboard limiter and therefore may pickup a level of D_α emission that is somewhat higher than the toroidal average. However, D_α monitored at two other toroidal locations during previous run campaigns has yielded comparable signals (within a factor of 2) under the same discharge conditions. This indicates that either toroidal asymmetry contributions are small or that the dominant contribution to the D_α signal comes from recycling at the inner-wall limiter surface. Profiles of Ly_α emission across the outer scrape-off layer are detected along 20 chords which view tangentially to magnetic flux surfaces[6]. The chords become tangent to magnetic flux surfaces at a location that is separated 30 cm toroidally from an outboard limiter, corresponding to the location of the D_α chords described above. Using a simple Abel inversion algorithm, the absolutely-calibrated brightnesses yield Ly_α emissivity profiles with 2 mm spatial resolution.

High resolution profiles of electron temperature and density across the separatrix and into the SOL are obtained from a combination of edge Thomson scattering[7] and two scanning probe diagnostics. A vertical-scanning probe samples plasma at a position 'upstream' from the throat of the outer divertor, and a horizontal-scanning probe records conditions 10 cm above the midplane. Both probes employ four Langmuir probe elements: Two elements are used to continuously monitor floating potential profiles while the other two are operated in a voltage sweep mode to obtain densities and temperatures along the probe's trajectory. The latter two elements also record ion saturation current fluctuations and can be used to form a 'Mach probe pair'; the plasma flow parallel to the local magnetic field can be estimated from the ratio of ion saturation currents[8]. By integrating the poloidal projection of parallel Mach and *ExB* flows along the trajectory of the vertical scanning probe, the particle flux directed towards the outer divertor throat and baffle can be obtained. Plasma density, electron temperatures and ion fluxes across the divertor target and baffles are obtained from an embedded array of Langmuir probes.

Profile data from all diagnostics are mapped onto magnetic flux surfaces and labeled by the coordinate ρ, which is defined as the distance in major radius outside the last-closed flux surface at

the outboard midplane. The electron stagnation pressure profiles measured by divertor probes, scanning probes, and edge Thomson scattering system can be made to overlay by adjusting their relative flux surface mappings in ρ. The technique is employed in this paper, to 'align' the data from these diagnostics with an estimated accuracy of ~2 mm. In any case, the principal results presented in this paper are not sensitive to mapping corrections. For example, D_{eff} estimates rely on the known locations of the horizontal-scanning probe and Ly_α chords and not the identification of the flux surface that is the separatrix.

III. PARTICLE BALANCE

A. Main-chamber recycling in Alcator C-Mod

A simple analysis of particle balance in Alcator C-Mod clearly shows that under a wide variety of discharge conditions, recycling in the main-chamber scrape-off layer (SOL) is predominately onto main-chamber surfaces. Particle fluxes to main-chamber surfaces are clearly large compared to the particle flow between the main-chamber and divertor volumes and can even exceed the particle flux onto the divertor target[2,3]. We summarize here some of the observations which support this picture. Further observations and details can be found in Refs. [2,3,11,12].

Figure 2 displays ion fluxes inferred from a variety of diagnostics versus line-averaged plasma density for a set of ohmic L-mode discharges (studied in more detail in section III). The vertical axis records: (1) ionization source in the main-chamber from midplane D_α brightness (a rough estimate of the total neutral flux 'attacking' the plasma in the main chamber) based on 45 ionizations per D_α photon[9] and assuming toroidal/poloidal symmetry, (2) ion flux onto the divertor target plus baffles, (3) ion flux onto the divertor baffles, (4) ion flux crossing a magnetic flux surface which is 4 to 5 mm beyond the shadow cast by the main-chamber limiters [from 'limiter shadow particle flux probe' (LSFP) assuming toroidal/poloidal transport symmetry], and (5) an estimate of the plasma flux heading toward the divertor throat and baffles based on vertical scanning probe data. The latter quantity includes Mach and *ExB* flows evaluated along the trajectory of the vertical scanning probe, multiplied by a factor of two to estimate the contribution from the inner

divertor leg (although *ExB* flows are likely to be pointing *away* from the divertor on this leg, possibly resulting in a lower value).

We assess the level of confidence in these estimates as follows. Based on camera images of visible light in the main chamber and on comparisons of data from the D_α and Ly_α diagnostics, we find evidence of a higher level of recycling (factor of 2 to 3) occurring on the smaller major radius edge of the plasma (inner limiter) than at the outer edge. This may be real or an artifact of these diagnostics not 'seeing' the full extent of the recycling from the outer limiters which might be highly localized. This observation, combined with the possibility of contributions of reflected light to the D_α measurement, suggest that the D_α estimate may be systematically high by a factor of ~2.

The ion fluxes to the divertor targets and baffles are based on a direct measurement of the ion saturation current density from probes and the assumption of toroidal symmetry of plasma conditions. The expected accuracy of these flux estimates is around ±20%, reflecting the uncertainty in the local current density measurements.

The local cross-field ion flux density entering into the shadow cast by the main-chamber limiters at the same poloidal location has been measured at two different toroidal locations by two different methods (horizontal scanning probe profiles in Ref. [3], LSPF data shown in Fig. 2). These two measurements agree quite well (±20%). In addition, cross-field integration of the Ly_α-derived ionization profile (discussed in next section) yields a separate estimate of the local ion flux density crossing a flux surface tangent to the main-chamber limiter edge. This value is systematically 0.5 times the flux density inferred from the LSFP over the full range of plasma conditions. These tests lend confidence that the Ly_α-derived local ionization profile estimates are indeed proportional to the local fluxes but that they may be systematically low by a factor of ~2.

If one accepts that recycling on the inner limiter is indeed higher than on the outer limiters by a factor of 2 to 3, then in order to get an estimate of the *total ion flux to all limiters*, one may need to multiply the LSPF estimate shown in Fig. 2 by a factor of 2 or more, particularly in view of the fact that the estimate shown here is based on the flux measured 4 to 5 mm beyond the shadow

cast by the limiters. Such an estimate of the *total ion flux to all limiters* would be in rough agreement with the main-chamber ionization source estimated from midplane D_α, reduced by a factor of ~2 to be consistent with the postulated in-out asymmetry.

Recognizing that there may be a significant in-out limiter recycling asymmetry, we use the LSPF estimate shown in Fig.2 as a lower-bound estimate of the *total ion flux to all limiters* in this paper. Further evidence that this quantity may under-represent the recycling fluxes on main-chamber limiter surfaces comes from a comparison of the neutral pressure measurements separated poloidally (and toroidally). A pressure gauge at the top of the vessel almost always measures pressures significantly above (x2-10) that measured at the midplane, suggesting a level of neutral pressure (recycling) surrounding the core plasma that may be minimum at the outer midplane.

Estimates of the plasma flux heading toward the divertor throat and baffles rely on Mach probe theory and accurate measurement of the *ExB* flows. We expect the accuracy here to be within about a factor of 2. It should be noted that the flux directed towards the divertor throat (not shown here) is only a portion (less than ~1/2) of the flux directed toward the divertor throat plus baffles.

Even allowing for the expected uncertainties in the flux estimates, Fig. 2 clearly illustrates the main-chamber recycling behavior in Alcator C-Mod over a wide range of discharge conditions ($0.14 < \bar{n}_e / n_G < 0.43$, with n_G being the Greenwald density[10]): The recycling onto main-chamber limiters is at least comparable (from limiter-shadow flux estimate) or greatly exceeds (from ionization source estimate) the ion flux arriving on the divertor target plus baffles. Flux directed towards the divertor throat is clearly much smaller than the ion flux arriving on the divertor targets. Thus, while a strong level of recycling occurs in both the divertor and main-chamber volumes there appears to be a relatively weak flux of particles communicating between them.

The physics underlying the magnitude of MCR in Alcator C-Mod and the degree to which other tokamaks exhibit similar phenomena is an interesting and important topic[11]. Clearly, in order to predict when or if a similar regime will occur in a tokamak reactor, one needs to develop a fundamental understanding of cross-field particle transport. If cross-field particle transport is

sufficiently high, then there can exist a situation where MCR will persist for virtually any divertor, baffle, and main-chamber wall geometry[3]. In this paper, we do not explore MCR further than in Ref [3]. Rather, we use the observation that C-Mod operates in the MCR regime to help extract some fundamental information about the relationship between cross-field particle transport, heat convection and the plasma conditions that exist in the SOL.

B. D_{eff} profiles from local particle balance

In the MCR regime, the outward, cross-field particle flux over the entire SOL is balanced primarily by ionization of neutrals evolving from main-chamber limiter/wall surfaces. As indicated in the previous section, parallel flows to distant divertor throat and baffles do not greatly influence this particle balance. Therefore, if one can obtain an estimate of the ionization profile across the SOL, then one can simply integrate it to estimate the cross-field particle flux density profile. Dividing the local cross-field particle flux density by the magnitude of the local density gradient leads to an estimate of an effective particle diffusion coefficient, D_{eff}.

At present, we do not measure the ionization profile over the entire 2-D domain of the SOL. However, we can compute the cross-field ionization profile at the poloidal location of the Ly_α diagnostic using Abel-inverted emissivity profiles, the density and temperature profiles measured by the horizontal-scanning probe, and Johnson-Hinnov rate coefficients[9]. Although we expect some degree of poloidal and/or toroidal asymmetry in the neutral densities surrounding the core plasma, we also expect the shape of the 'poloidally averaged' ionization profile, which is determined by neutral charge exchange and ionization, to be similar to the locally inferred ionization profile. Therefore, in the MCR regime, we expect the cross-field particle flux profile to be approximately proportional to the integral of the local cross-field ionization source profile. The degree to which the ionization profile at the location of the Ly_α diagnostic is characteristic of the poloidally averaged ionization profile and the influence of parallel flows to the divertor and baffle structure on the inferred cross-field flux profile can be assessed with the help of 2-D transport simulations.

This method for estimating cross-field particle flux and D_{eff} profiles directly from the Ly_α-

inferred ionization profiles, including the effect of plasma flows toward the divertor throat and baffles was examined in Ref [3]. The method was found to systematically track cross-field fluxes and D_{eff} profiles within a factor of ~2 of that obtained from full 2-D transport simulations[12] using UEDGE[13] over a wide variation in plasma density, with a tendency towards reporting lower D_{eff} values. A sensitivity study was also reported in Ref [3], varying the plasma flow toward the divertor throat and baffles over the values of 0, 0.5 and 1.0 times the flux arriving on the limiters/wall. In changing this parameter (α) from 0.5 to 1.0, (the value estimated from measurements is α ~0.5) the cross-field fluxes and D_{eff} values near the separatrix correspondingly increase by a factor of 2 while these values at the limiter edge are unaffected, being fixed by the flux arriving at the limiters/wall (which, in turn, must be consistent with midplane neutral pressures, Ly_α-derived ionization profile, and limiter flux probe measurements). In the remainder of this paper, results are reported using the parameter α = 0.5, which, as seen in the UEDGE simulations, may lead to an underestimate of cross-field fluxes and D_{eff} values near the separatrix.

Figure 3 shows D_{eff} profiles extracted by this analysis technique for three 0.8 MA discharges with different line-averaged densities: (a) $\bar{n}_e = 1.1 \times 10^{20}$ m^{-3}, (b) $\bar{n}_e = 1.6 \times 10^{20}$ m^{-3}, and (c) $\bar{n}_e = 2.6 \times 10^{20}$ m^{-3}. A number of important characteristics can be seen in this sequence:

- The density profile exhibits a two-layer structure: a steep exponential decay near the separatrix and a much more gradual exponential decay in the far SOL. As the plasma density is raised, density profiles flatten everywhere.
- The ionization profile behaves as expected; as the density is raised, it strongly increases in magnitude and tends to peak further out into the SOL.
- The inferred cross-field plasma flux density is flat or slightly increasing across the SOL. Its magnitude also strongly increases with plasma density.
- The resultant D_{eff} profiles dramatically increase with distance into the SOL. The primary

reason for this inferred increase is the variation of the density gradient across the profile; the flux profile is mostly flat. D_{eff} increases nearly everywhere with increasing $\bar{n}_e$.

- In the far SOL, D_{eff} is clearly a poor characterization of the transport process; the density gradient becomes nearly flat [case (c)] yet the cross-field flux remains very large.

It is important to emphasize that this behavior of particle transport is radically different than the constant particle diffusion coefficient that is often assumed in 2-D numerical simulations of the SOL. With a constant particle diffusion coefficient, the density profile would need to get steeper as the main-chamber wall is approached in order to drive an increasing cross-field particle flux. Clearly, the ~exponential decay of density with distance into the C-Mod SOL is a consequence of a rapid spatial increase in D_{eff}. (Our use of the term 'D_{eff}' here is not meant to imply that the transport is uniquely related to local conditions and the local density gradient. Rather, it is simply the diffusion coefficient that would be required to yield the observed fluxes. For example, it is possible that local transport could be dominated by large scale convection cells set by non-local conditions.) It should also be noted that the ~exponential density profile decay is not evidence of, nor is it caused by, a preponderance of particles streaming along field lines, exhausting into the divertor volume or onto divertor baffle surfaces.

IV. PARTICLE AND HEAT TRANSPORT DEPENDENCIES

A. D_{eff} correlations

An advantage of the above technique is that it can be performed in many discharges, allowing correlations of D_{eff} with local or global conditions to be identified. Recently, a clear correlation between the local values of D_{eff} and the local values of density and electron temperature in the near SOL has been reported for a set of ohmic L-mode discharges with different core densities[3], suggesting the relationship: $D_{eff} \sim \lambda_{ei}^{-1.7}$, where λ_{ei} is the electron-ion mean-free path. Here we apply the same analysis to a more recent set of discharges which included differing plasma

currents (I_p) and toroidal magnetic fields (B_T): $0.6 < I_p < 1.0$ MA, $4 < B_T < 6$ tesla, $0.8\text{x}10^{20} < \bar{n}_e < 2.5\text{x}10^{20}$ m^{-3}, yielding 64 time-slices with normalized density range, $0.14 < \bar{n}_e / n_G < 0.47$.

Fig. 4 shows regression analyses results, correlating D_{eff} at $\rho = 2$ mm with 3 different sets of regressors: (a) T_e and n at $\rho = 2$ mm, I_p, and B_T, (b) T_e and λ_{ei}/L at $\rho = 2$ mm (Here, L is the local magnetic field line length connecting from inner to outer divertor target/baffle, divided by two), and (c) λ_{ei}/L at $\rho = 2$ mm. Table I also presents analysis at $\rho = 4$ and 6 mm locations and includes partial F-test statisitics of the regressors (columns labeled '-test') and the square of the multiple correlation coefficients (R^2)[14]. As seen in Table I, partial F-tests and multiple correlation coefficients using data from the far SOL ($\rho \geq 6$ mm) are low. The analysis therefore does not offer reliable information about trends in D_{eff} in this zone. However, a number of important trends can be inferred about D_{eff} in the near SOL:

- The four-parameter regression (T_e, n, I_p, and B_T) suggests a rough B_T/I_p dependence of D_{eff} . One could consider this a q (safety factor) dependence or a dependence on the parallel magnetic connection length, L.
- The two parameter regression (T_e, λ_{ei}/L) does just as well statistically, implying that the dependence on L (or q) is well represented in λ_{ei}/L. Partial F-test values indicate that λ_{ei}/L is more important than T_e.
- The single-parameter regression ($0.014 < \lambda_{ei}/L < 0.14$) does almost as well as the multi-parameter regressions with partial F-test values for λ_{ei}/L being higher than any other parameter. This identifies λ_{ei}/L is the most statistically relevant parameter. Apart from the newly found dependence on the parameter, L, the implied relationship at $\rho = 2$ mm, $D_{eff} \sim (\lambda_{ei}/L)^{-1.7}$, is identical to that reported previously[3].

B. Cross-field heat convection

The regression analysis suggests that as λ_{ei}/L decreases, cross-field particle transport in the near SOL increases. Ionization profiles (e.g., Fig. 3) indicate that cross-field particle flux densities ($\Gamma_\perp$) remain roughly at the same level or higher as they traverse the far SOL. It is interesting to compare the resultant convected power crossing a given flux surface (Q_{conv}) to the power that must cross that flux surface (Q_{div}) in order to support parallel electron conduction losses to the divertor target and baffles. Assuming $T_i \approx T_e$, the convected power is $Q_{conv} \sim A_{LCFS}$ $5\, T_e\, \Gamma_\perp$. The parallel heat flux arising from electron conduction is $q_{//} = -\frac{2}{7}\kappa_0 \nabla_{//} T_e^{7/2}$ with $\kappa_0 \approx$ $2.8\text{x}10^3$ in units of watts m^{-1} $\text{eV}^{-7/2}$. Assuming a T_e profile along the field line that is symmetric with respect to the divertor targets, an equivalent uniform volumetric heat loss along the length of the field line can be constructed, $S = \nabla_{//} \cdot q_{//} \approx \frac{4}{7\pi^2 R^2 q^2}\kappa_0 (T_0^{7/2} - T_w^{7/2})$, where q is the safety factor (evaluated at 95% flux surface), R is major radius, T_0 is the peak electron temperature on the field line ($\approx T_e$ measured by horizontal probe) and T_W is the temperature at the divertor/baffle surface. An estimate of the cross-field power necessary to support electron parallel conduction losses in the SOL beyond the flux surface at location ρ can therefore be obtained by integrating S over the volume between that flux surface and the one tangent to the limiter,

$$Q_{div}(\rho) \approx A_{LCFS}\, \frac{4}{7} \frac{\kappa_0}{\pi^2 R^2 q^2} \int_{\rho}^{\rho_{\text{limiter}}} T_0^{7/2}\, \partial\rho', \qquad (1)$$

where A_{LCFS} is the area of the last closed flux surface. Equation (1) may be considered an upper estimate since it effectively sets T_W to be zero.

Figure 5 shows the density and electron temperature profiles from two discharges (lowest and highest density discharges shown previously in Fig. 2) along with the corresponding estimates

of Q_{conv} and Q_{div}. Some important characteristics are made evident by this comparison:

- In both discharges, Q_{conv} exceeds Q_{div} in the far SOL (ρ > 7 mm); parallel electron conduction is not high enough to handle the power entering this region. Since these discharges exhibit MCR, we already know that parallel heat convection to the divertor target and baffles is not significant relative to cross-field heat convection. Therefore, cross-field heat convection combined with an undetermined amount of cross-field conduction, charge exchange, and radiation to the main-chamber walls must be dominating the heat losses in this region.
- In the lower density discharge, Q_{conv} by itself can not account for Q_{div} in the near SOL (ρ < 7 mm). This implies that a significant level of cross-field heat conduction must be active in this zone. Moreover, since Q_{conv} is small relative to Q_{div}, it appears that the electron temperature profile in this zone is primarily governed by the cross-field heat diffusivity and parallel conduction loss to the divertor. In this regime, one expects the temperature at the separatrix (T_{sep}) to be more or less fixed, satisfying the well-known relationship[15] with power into the SOL (P_{sol}), $T_{sep} \propto P_{sol}^{2/7}$.
- In the higher density discharge, Q_{conv} exceeds Q_{div} over the entire SOL; cross-field heat transport to the main-chamber walls is now dominating the heat losses over the entire SOL.

The above observations suggest the following picture: As the plasma density is raised (or more generally, λ_{ei}/L near the separatrix reduced) cross-field particle transport increases and heat losses from cross-field transport become more important than heat losses from parallel electron conduction over an increasingly larger portion of the SOL, starting with the far SOL. Apparently, for sufficiently low values of λ_{ei}/L near the separatrix, electron parallel conduction losses no longer regulate the magnitude or shape of the electron temperature profile anywhere in the SOL.

C. SOL Power Balance

As a test of the confidence level in the $Q_{conv}(\rho)$ and $Q_{div}(\rho)$ estimates, we can evaluate these quantities at the separatrix and compare them to independent estimates of the total power flowing into the SOL (P_{sol}, based on input power minus core radiation) and the total power convected to the main-chamber limiters (P_{lim}, based on $5\ T_e$ times the particle flux to the main-chamber limiters, estimated from the limiter flux probe). These quantities are plotted as a function of $\bar{n}_e / n_G$ in Fig. 6 for the same set of discharges shown in Fig. 2.

We see that at low density, the estimate of power conducted to the divertor approximately balances the power crossing the LCFS. This gives us some assurance that the conduction estimate is roughly right. As the density is raised, the power conducted to the divertor can not account for the power into the SOL. However, according to the limiter flux-probe estimate, the power convected to the main-chamber limiters rises strongly with density. The sum of Q_{div} and P_{lim} approximately accounts for the power into the SOL. The quantity $Q_{conv}(0)$, which is derived independently, also tracks P_{lim} very well but it may be systematically low (or P_{lim} systematically high) since one would expect $Q_{conv}(\rho_{limiter})$ to be lower than $Q_{conv}(0)$ (as shown in Fig. 5) and $Q_{conv}(\rho_{limiter})$ to be comparable or greater than P_{lim} (and remembering that P_{lim} is computed at a location ~4 mm in the shadow of the main-chamber limiters). In any case, these data clearly support the conclusion that as the discharge density is raised the heat conducted to the divertor falls and the heat convected to the main-chamber walls increases. Also, the heat flux estimates appear to be sufficiently accurate to conclude that cross-field heat convection dominates over parallel conduction losses over the entire SOL for $\bar{n}_e / n_G >$ ~0.45. Possible additional heat losses from cross-field heat conduction, charge exchange, and SOL radiation not seen by the core bolometer diagnostic are not considered here.

V. PLASMA FLUCTUATIONS AND BEHAVIOR NEAR DENSITY LIMIT

A. Character of fluctuations across the SOL

The underlying physics of cross-field particle and heat transport involves plasma turbulence. Therefore, one expects some correspondence to exist between the character of plasma fluctuations and the observed transport. As discussed here, a clear correspondence is indeed detected, consistent with different particle and heat transport physics in the near and far SOL.

The top panel in Fig. 7 shows a typical cross-field plasma density profile from the horizontal scanning probe. Subsequent panels show time snapshots of ion saturation current (I_{sat}) normalized to the mean values recorded by the probe as it traverses the SOL. In the near SOL region, where the gradients are large, the fluctuation amplitude is the lowest and the data exhibit a steady stream of apparently random fluctuations. At the location where the density gradient noticeably flattens (ρ ~ 5 mm) the fluctuations also noticeably change. From this location and outward into the SOL the data exhibit lower-frequency, higher-amplitude fluctuations with intermittent, long-lived 'bursts' of ion saturation current arriving at the probe.

The lifetime of 'bursts' in ion saturation current at a given location can be quantified by the auto-correlation time. At any location in the SOL the auto-correlation function (not shown) drops more or less exponentially with a characteristic e-folding time (τ). However, the values of τ indicated in Fig. 7 show that the 'bursts' in ion saturation current last systematically longer as the distance from the separatrix increases.

B. Behavior as density limit is approached

Up to this point, we have been focussing on SOL transport and turbulence characteristics in discharges with $\bar{n}_e$ less than 0.47 times the Greenwald limit (n_G)[10]. An interesting behavior unfolds as the discharge density approaches n_G.

Figure 8 shows the time history of a typical discharge used to for this study: An ohmic L-mode discharge with a continuously ramping plasma density is established by gas puffing. After a period of ~0.7 seconds, the plasma current is ramped down such that a density limit induced

disruption occurs. The middle panel in Fig. 8 displays the total input power (ohmic), total radiated power (2π bolometer), and an estimate of the power convected through a magnetic flux surface in the shadow of the main-chamber limiters (based on $5\ T_e$ + 13.6 times the particle flux to the main-chamber limiters, estimated from the limiter flux probe). These traces display that the sum of radiation and limiter convection losses account for almost all the input power as the density limit is approached. The density limit is reached near the time when these losses exceed the input power. The horizontal scanning probe is used to record SOL profiles at three times when $\bar{n}_e / n_G$ = 0.34, 0.41, and 0.82. The corresponding values of λ_{ei}/L at ρ = 1 mm are indicated, showing a rapid reduction in this parameter near the separatrix as the density limit is approached.

Cross-field profiles of density (normalized to n_G), electron temperature, and fluctuation characteristics obtained by the horizontal probe are shown in Fig. 9. In general, the density and temperature profiles show a familiar flattening as the core density is raised (or λ_{ei}/L near separatrix reduced). However, for $\bar{n}_e / n_G$ ~ 0.8, there no longer is a transition between a steep-gradient region in the near SOL and a shallow gradient region in the far SOL. The 'break-point' in these regions appears to move toward the separatrix such that for the profile at $\bar{n}_e / n_G$ ~ 0.8 the 'break-point' is inside the separatrix! Moreover, the normalized density at the separatrix does not increase with $\bar{n}_e / n_G$ over this range but appears to saturate at a maximum value of ~0.2; large gradients in density and temperature must exist further inside closed flux surfaces in order to account for the core plasma densities and temperatures in this discharge.

The fluctuation profiles tell a similar story. At low $\bar{n}_e / n_G$, the auto-correlation times and the normalized ion saturation current fluctuation amplitudes show the usual behavior; they track with the density gradient, being lower in a steep-gradient 'near SOL' region and higher in a shallow-gradient 'far SOL' region. For the density profile at $\bar{n}_e / n_G$ ~ 0.8 there is no steep gradient region in the SOL, and correspondingly, the auto-correlation times and the normalized ion saturation current fluctuation amplitudes are large across the entire SOL.

Thus it appears that the high cross-field transport zone (high D_{eff}), which is normally restricted to the far SOL region for low $\bar{n}_e / n_G$, envelops the entire SOL for high $\bar{n}_e / n_G$. This may explain why the normalized separatrix density becomes saturated at the value of ~0.2 and no longer increases with $\bar{n}_e / n_G$. As shown in Fig. 8, the magnitude of the cross-field heat convection to the walls at high $\bar{n}_e / n_G$ is large enough to impact the power balance of the discharge.

VI. DISCUSSION

Evidence for increased cross-field particle transport in the far SOL has been seen before in a number of other experiments. A 'shoulder' in the cross-field density and temperature profiles have been seen in ASDEX[16] and JT-60U[17]. This feature is found to persist regardless of changes in the divertor geometry[18,19]. In ASDEX-UG, the profiles in the shoulder region could be reproduced in simulations by assuming a large outward drift of 70 m s^{-1} or an effective particle diffusion coefficient much larger than Bohm of $D_{eff} \sim 30$ m^2 s^{-1} [16]. Also similar to Alcator C-Mod results[20-22], neutral pressures in the main-chamber of ASDEX-UG were unaffected in changing to a more closed divertor geometry[23] suggesting that rapid transport in the far SOL and subsequent wall recycling sets the neutral pressures in the main-chamber.

A recent investigation of helium transport in the Alcator C-Mod SOL with an ion mass spectrometer also indicates rapid cross-field transport in the far SOL[24]. It was found that in order to account for the relatively large ratio of singly- to doubly-charged ^{3}He ions arriving at the wall, the cross-field diffusive and/or convective transport of helium must increase with distance from the separatrix. Near the wall, the required effective particle diffusion coefficient exceeded the Bohm level by more than two orders of magnitude, implying that an outward particle convection model may be a more appropriate description of the transport process.

The overall characteristics of SOL plasma fluctuations seen in the C-Mod (frequency range,

$k_\perp \rho_i$ range, auto-correlation times, 'bursty' behavior) are ubiquitous features of turbulence in edge plasmas[25]. Similar to the results reported in this paper, experiments on ASDEX[26] found that lifetimes and correlation lengths (poloidal and radial) of H_α fluctuations increased with increasing line-averaged density at a fixed location in the SOL. In JET[27], a variation in the character of the turbulence with position in the SOL was seen; the frequency band over which turbulent transport fluxes occur varied from low frequencies in the SOL region to high frequencies inside the last-closed flux surface. This work also reported turbulent transport fluxes remaining approximately constant with distance into the SOL (within a factor of 2), despite almost an order of magnitude variation in the gradient of the ion saturation current (~density) profile. These results imply D_{eff} values increasing by nearly an order of magnitude with distance into the SOL.

Additional information on the character of the edge turbulence in Alcator C-Mod is presently being compiled through visible light emission measurements in the far SOL using a set of fast time-response diodes[28,29] and a high-resolution 2-D spatial imaging[30] of a localized gas puff. Visible light emission from 3 spatial locations in the far SOL separated by 3.4 mm indicate that 'bursts' in visible light emission have radial correlation lengths of ~7 mm and an effective propagation velocity towards the wall in excess of a few 100 m s^{-1}. Snapshots of 2-D images of visible light emission with 2 μs exposure show intermittent, spatially separated 'blobs' of emission in the far SOL. Isolated blobs, which are viewed along magnetic field lines by optics, have a roughly circular form with a characteristic size of about 10 mm in diameter. Blobs are often seen extending across the far SOL, into the shadow of the main-chamber limiters. The 'bursts' seen in probe and fast-diode data combined with the 'blobs' seen in the 2-D imaging data are consistent with the idea that large density and perhaps temperature perturbations propagate across the far SOL, convecting particles and energy to the main-chamber limiters.

As outlined by Wesson[31], a density limit disruption is believed to involve the onset of a thermal instability in which the edge plasma cools and the current channel shrinks, becoming magneto-hydrodynamic (MHD) unstable. Impurity radiation by itself can drive such a thermal

instability when the radiated power becomes equal to the input power. However, as pointed out in Ref.[10], a thermal collapse could also arise from cross-field transport in the plasma edge; if transport increases rapidly in response to a cold plasma edge, then a thermal instability can ensue. In this scenario, radiation could act in concert with transport to establish a thermal instability or radiation could act as an intermediary, carrying power from a large volume of cold halo plasma to the wall. The observations outlined in this paper lend support to this more generalized scenario; particle transport across the separatrix in Alcator C-Mod increases as the edge plasma becomes more collisional; as the density limit is approached, heat convection onto the wall impacts the power balance of the discharge. Thus, particle transport and heat convection in the edge plasma and its scaling with discharge parameters may be a key physics element underlying the empirical scaling of the tokamak density limit.

VII. SUMMARY

Owing to rapid cross-field particle transport, Alcator C-Mod operates predominately in a 'main-chamber recycling regime' where particle fluxes to main-chamber surfaces are large compared to the particle flow between the main-chamber and divertor volumes and can even exceed the particle flux onto the divertor target. Taking advantage of particle balance in this regime, effective particle diffusion coefficients profiles (D_{eff}) can be estimated directly from ionization profiles. D_{eff} is found to increase dramatically with distance into the SOL. The shape of the density profile is primarily responsible for this inference: A steep density gradient typically exists in the near SOL (~ 5 mm from separatrix) while a shallow gradient exists outside this region; the cross-field particle flux profile is relatively flat. D_{eff} in the near SOL is found to be well correlated with local electron-ion mean-free path (λ_{ei}) normalized to local magnetic connection (L), $D_{eff} \sim (\lambda_{ei}/L)^{-1.7}$, over a range of plasma densities ($0.14 < \bar{n}_e / n_G < 0.47$). As λ_{ei}/L is decreased, cross-field heat convection becomes larger than parallel heat losses to the divertor over an increasing portion of the SOL.

Consistent with the observation that D_{eff} increases with distance from the separatrix, the amplitude and character of plasma fluctuations in the near and far SOL zones is markedly different: Moderate fluctuation amplitudes are associated with the steep gradients in the near SOL while larger fluctuation levels and longer correlation times are associated with the smaller gradients in the far SOL. In discharges which approach the density limit, λ_{ei}/L near the separatrix becomes very small, D_{eff} becomes large, the plasma density at the separatrix no longer increases, and fluctuations which were previously characteristic of the far SOL now occur even across the separatrix.

Above $\bar{n}_e / n_G \sim 0.5$, cross-field heat convection clearly dominates over parallel conduction losses over the entire SOL. Thus, as the density limit is approached, the electron temperature near the separatrix is not regulated by parallel conduction to be an approximately fixed value ($T_{sep} \propto P_{sol}^{2/7}$). Instead, the level of anomalous cross-field heat convection impacts the temperature at the separatrix and becomes an important component in the power losses of the discharge. These observations suggest that the particle and heat transport physics of the edge plasma may play a key role in determining the maximum density that can be sustained in a tokamak discharge.

Acknowledgements

These results were made possible by the excellent engineers, technical staff, students, and scientists on the Alcator team. This work is supported by U.S. Department of Energy Coop. Agreement DE-FC02-99ER54512.

References

[1]I. H. Hutchinson, R. Boivin, F. Bombarda *et al.*, Phys. Plasmas **1**, 1511 (1994).

[2]M. V. Umansky, S. I. Krasheninnikov, B. LaBombard *et al.*, Phys. Plasmas **5**, 3373 (1998).

[3]B. LaBombard, M. V. Umansky, R. L. Boivin *et al.*, Nucl. Fusion **40**, 2041 (2000).

[4]M. Greenwald, R. Boivin, P. Bonoli *et al.*, Phys. Plasmas **6**, 1943 (1999).

[5]A. Hubbard, Bull. Amer. Phys. Soc. **45**, 17 (2000).

[6]R. L. Boivin, J. A. Goetz, A. E. Hubbard *et al.*, Phys. Plasmas **7**, 1919 (2000).

[7]J. W. Hughes, D. A. Mossessian, A. E. Hubbard *et al.*, "High resolution edge Thomson scattering measurements on the Alcator C-Mod tokamak", to be published in Rev. Sci. Instrum.

[8]I. H. Hutchinson, Phys. Fluids **30**, 3777 (1987).

[9]L. C. Johnson and E. Hinnov, J. Quant. Spectrosc. Radiat. Transfer **13**, 333 (1973).

[10]M. Greenwald, J. L. Terry, S. M. Wolfe *et al.*, Nucl. Fusion **28**, 2199 (1988).

[11]B. LaBombard, J. A. Goetz, B. Lipschultz *et al.*, "Cross-Field Transport in the SOL: Its Relationship to Main Chamber and Divertor Neutral Control in Alcator C-Mod," in *18th IAEA Fusion Energy Conference* (International Atomic Energy Agency, Vienna, 2000), pp. IAEA-CN-77-EXS/76, to be published.

[12]M. V. Umansky, S. I. Krasheninnikov, B. LaBombard *et al.*, Phys. Plasmas **6**, 2791 (1999).

[13]T. D. Rognlien, J. L. Milovich, M. E. Rensink *et al.*, J. Nucl. Mater. **196-198**, 347 (1992).

[14]Philip R. Bevington, *Data reduction and error analysis for the physical sciences* (McGraw-Hill, New York, 1969).

[15]P. C. Stangeby, *The plasma boundary of magnetic fusion devices Peter C. Stangeby* (Institute of Physics Pub., Bristol, UK ; Philadelphia, PA, 2000).

[16]K. McCormick, S. Fiedler, G. Kyriakakis *et al.*, "Particle and Energy Transport in the ASDEX Scrape-Off Layer," in *Controlled Fusion and Plasma Physics* (European Physical Society, Geneva (1993), Lissabon, 1993), Vol. 2, pp. 597.

[17]N. Asakura, Y. Koide, K. Itami *et al.*, J. Nucl. Mater. **241-243**, 559 (1997).

[18]H. S. Bosch, J. Neuhauser, R. Schneider *et al.*, J. Nucl. Mater. **220-220**, 558 (1995).

[19]N. Asakura, N. Hosogane, K. Itami *et al.*, J. Nucl. Mater. **266-269**, 182 (1999).

[20]C. S. Pitcher, C. J. Boswell, T. Chung *et al.*, "The Effect of Baffling on Divertor Leakage in Alcator C-Mod ", to be published in J. Nucl. Mater.

[21]B. LaBombard, J. A. Goetz, I. Hutchinson *et al.*, J. Nucl. Mater. **241-243**, 149 (1997).

[22]C. S. Pitcher, C. J. Boswell, J. A. Goetz *et al.*, Phys. Plasmas **7**, 1894 (2000).

[23]H. S. Bosch, W. Ullrich, A. Bard *et al.*, J. Nucl. Mater. **266-269**, 462 (1999).

[24]R. Nachtrieb and B. LaBombard, Phys. Plasmas **7**, 4573 (2000).

[25]M. Endler, J. Nucl. Mater. **266**, 84 (1999).

[26]M. Endler, H. Niedermeyer, L. Giannone *et al.*, Nucl. Fusion **35**, 1307 (1995).

[27]I. Garcia-Cortes, R. Balbin, A. Loarte *et al.*, Plasma Phys. Control. Fusion **42**, 389 (2000).

[28]J. L. Terry, R. Maqueda, S. J. Zweben *et al.*, "Visible Imaging of Edge Turbulence in the Alcator C-Mod Tokamak", to be published in J. Nucl. Mater.

[29]J. L. Terry, B. LaBombard, C. S. Pitcher *et al.*, Bull. Amer. Phys. Soc. **45**, 320 (2000).

[30]S. J. Zweben, R. Maqueda, J. Terry *et al.*, Bull. Amer. Phys. Soc. **45**, 188 (2000).

[31]J. A. Wesson, R. D. Gill, M. Hugon *et al.*, Nucl. Fusion **29**, 641 (1989).

Table I –Regression analysis: Correlation of D_{eff} measured at three spatial locations (ρ)

ρ(mm)	D_{eff}^*	α	β	γ	δ	ε	T_e-test	n-test	I_p-test	B_T-test	λ_{ei}/L-test	R^2
2	0.029	-3.8	1.1	- 1.2	1.8		107	43	16	11		0.80
2	0.0014	-1.5				-1.2	10				48	0.79
2	0.00052					-1.7					186	0.75
4	0.025	-4.3	0.9	- 1.3	1.5		130	48	29	9.0		0.80
4	0.0026	-2.4				-1.0	28				66	0.79
4	0.0024					-1.4					144	0.70
6	0.17	-1.5	1.0	- 1.4	0.2		4.6	21	15	0.03		0.40
6	0.018	0.3				-1.0	0.12				28	0.36
6	0.016					-1.0					36	0.36

$$D_{eff}\ (\mathrm{m^2\ s^{-1}}) = D_{eff}^*\ (T_e/50\ \mathrm{eV})^{\alpha}\ (n/10^{20}\ \mathrm{m^{-3}})^{\beta} (I_p/1\ \mathrm{MA})^{\gamma}\ (B_T/5\ \mathrm{tesla})^{\delta}\ (\lambda_{ei}/L)^{\varepsilon}$$

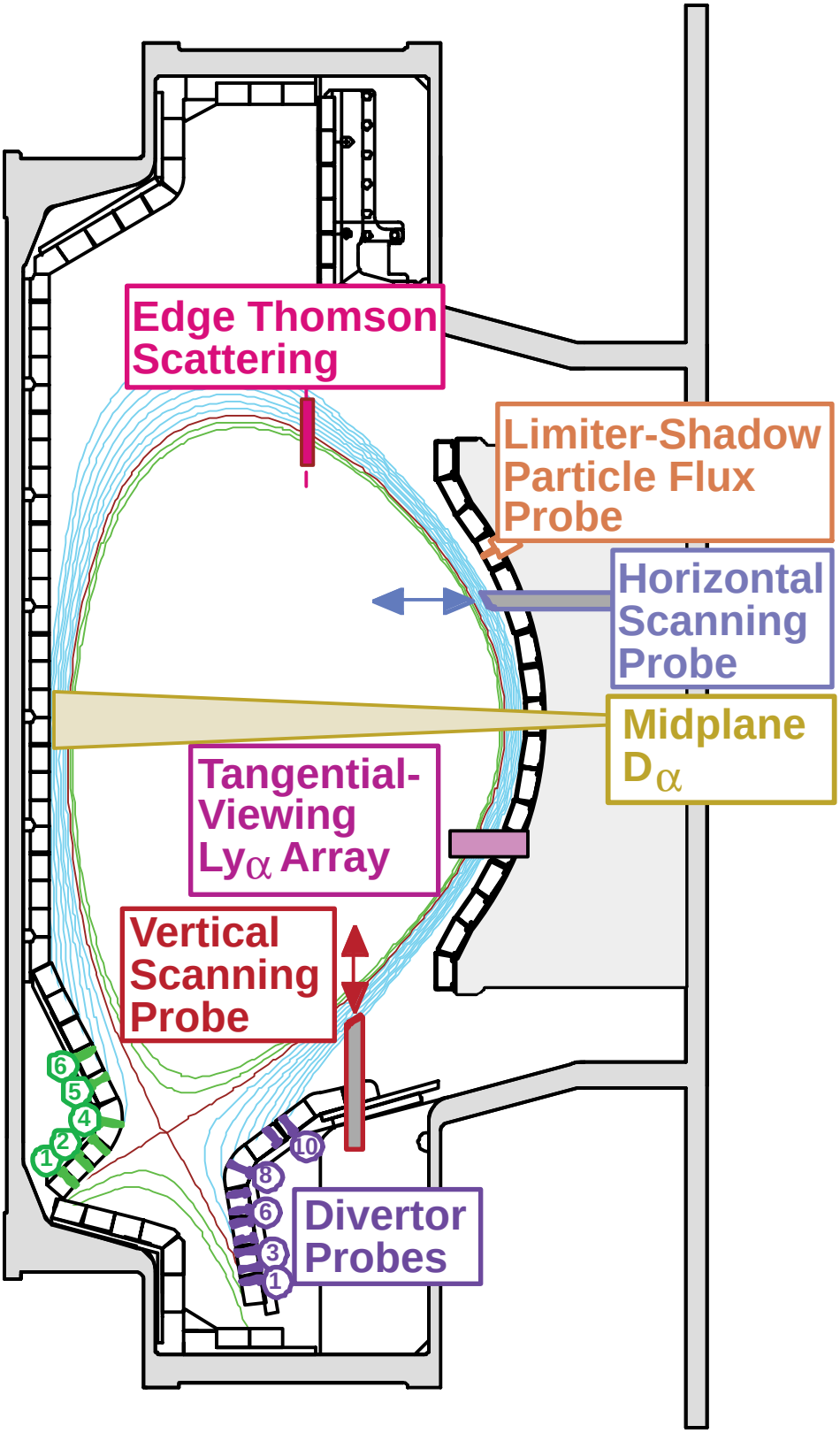

Fig. 1. Cross-section of Alcator C-Mod showing divertor geometry, edge plasma diagnostics and a typical plasma equilibrium used for these studies. Each magnetic flux contour corresponds to a $\Delta\rho$ = 2 mm radial separation at the midplane. In this paper, the separatrix is designated as ρ = 0 and the scrape-off layer as ρ > 0.

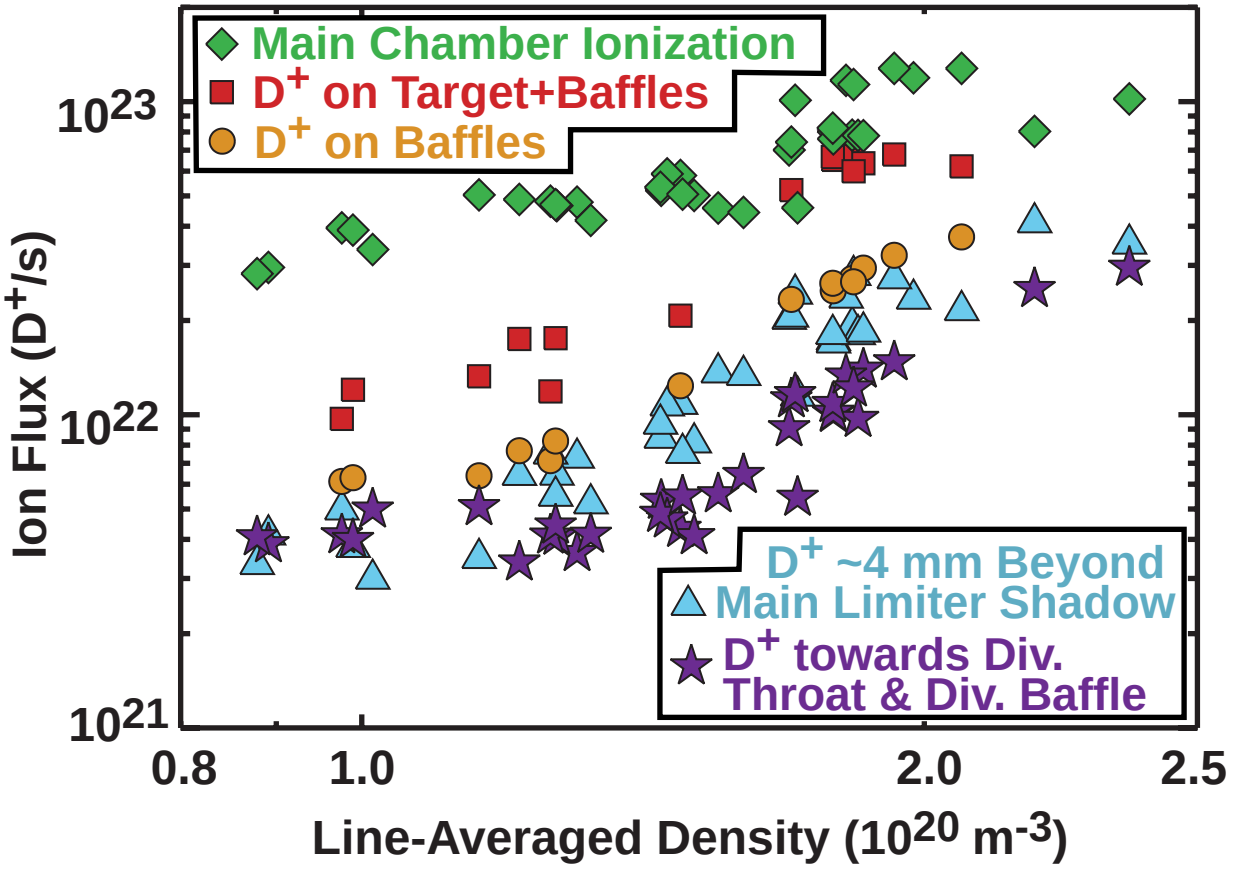

Fig. 2. Estimates of ion fluxes in C-Mod discharges. Vertical axis: (◆) ionization fluxes in the main chamber from midplane D_α, (■) ion fluxes onto divertor target plus baffles and (●) ion fluxes onto divertor baffles only from divertor probes, (▲) ion fluxes crossing a magnetic flux surface, 4 to 5 mm beyond the shadow of the main-chamber limiters, based on the limiter-shadow particle flux probe (see Fig.1), assuming toroidal/poloidal symmetry and (★) ion fluxes directed towards the divertor throat and baffles from vertical scanning Langmuir/Mach probe. Horizontal axis: line-averaged density of corresponding discharge.

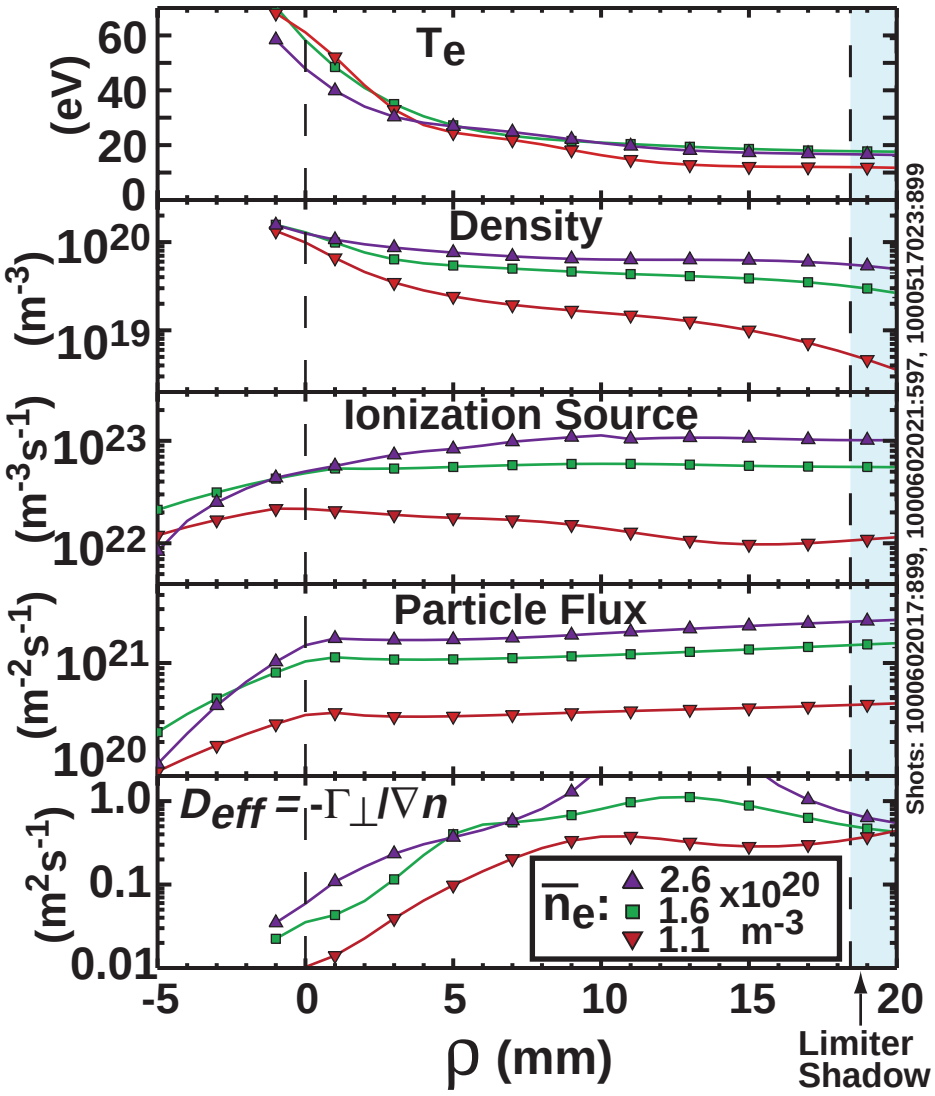

Fig. 3. Cross field profiles of electron temperature, plasma density (n), ionization source (S_{ion}, inferred from Ly$_\alpha$), and cross-field particle flux density ($\Gamma_\perp$) inferred from the integral of S_{ion}, using the method in Ref [3]. Data from discharges with three different line-averaged densities are shown: (▼) 1.1x10^{20} m^{-3}, (■) 1.6x10^{20} m^{-3}, and (▲) 2.6x10^{20} m^{-3}. Effective cross-field particle diffusivity profiles (D_{eff}) are computed from $\Gamma_\perp$ and ∇n.

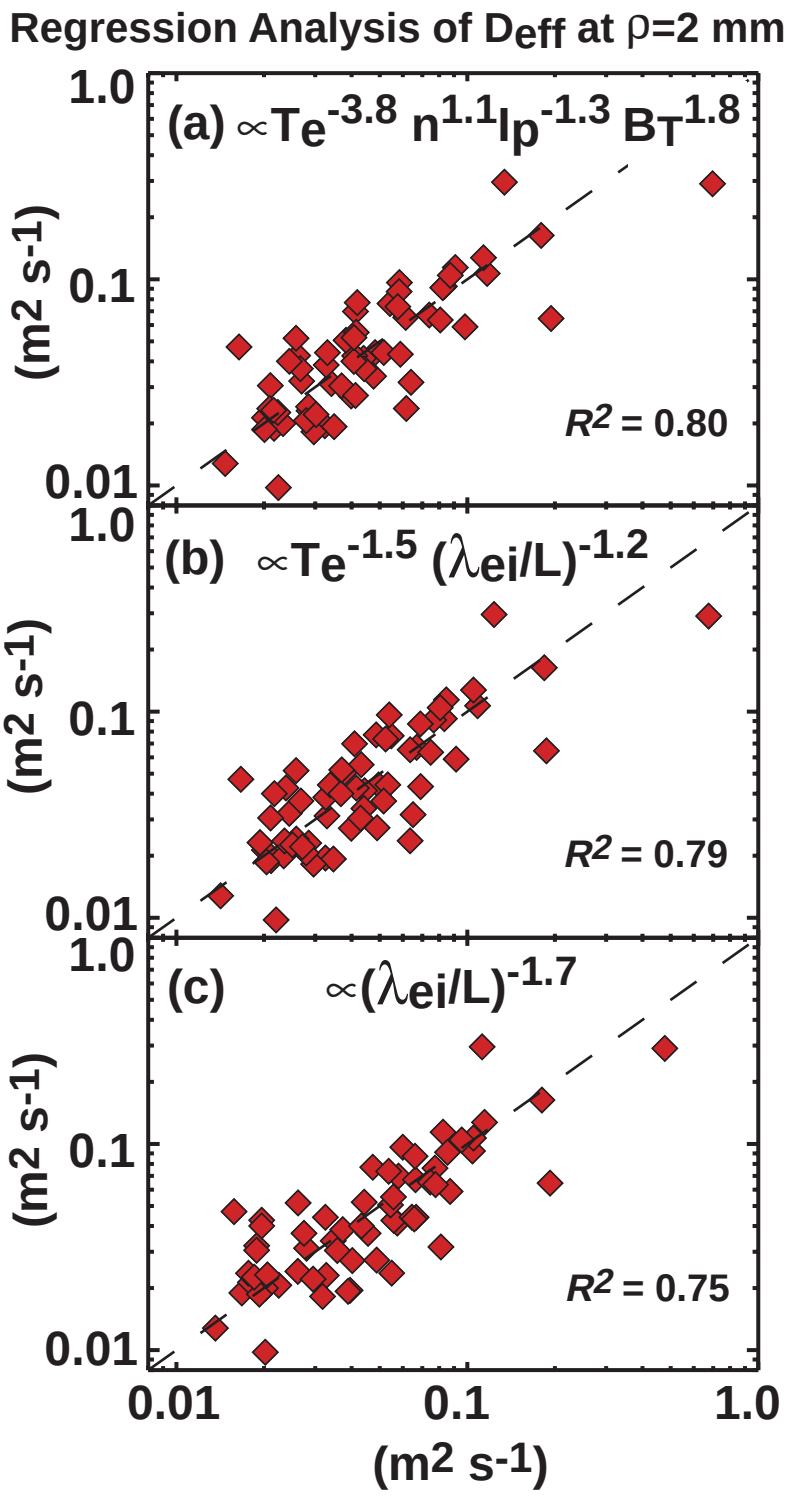

Fig. 4. Results of correlating D_{eff} at ρ = 2 mm with 3 different sets of regressors: (a) T_e and n at ρ = 2 mm, I_p, and B_T, (b) T_e and λ_{ei}/L at ρ = 2 mm, and (c) λ_{ei}/L at ρ = 2 mm. The regressions include 64 data samples, obtained in discharges with parameter range: $0.6 < I_p < 1.0$ MA, $4 < B_T < 6$ tesla, $0.8\text{x}10^{20} < \bar{n}_e < 2.5\text{x}10^{20}$ m^{-3}.

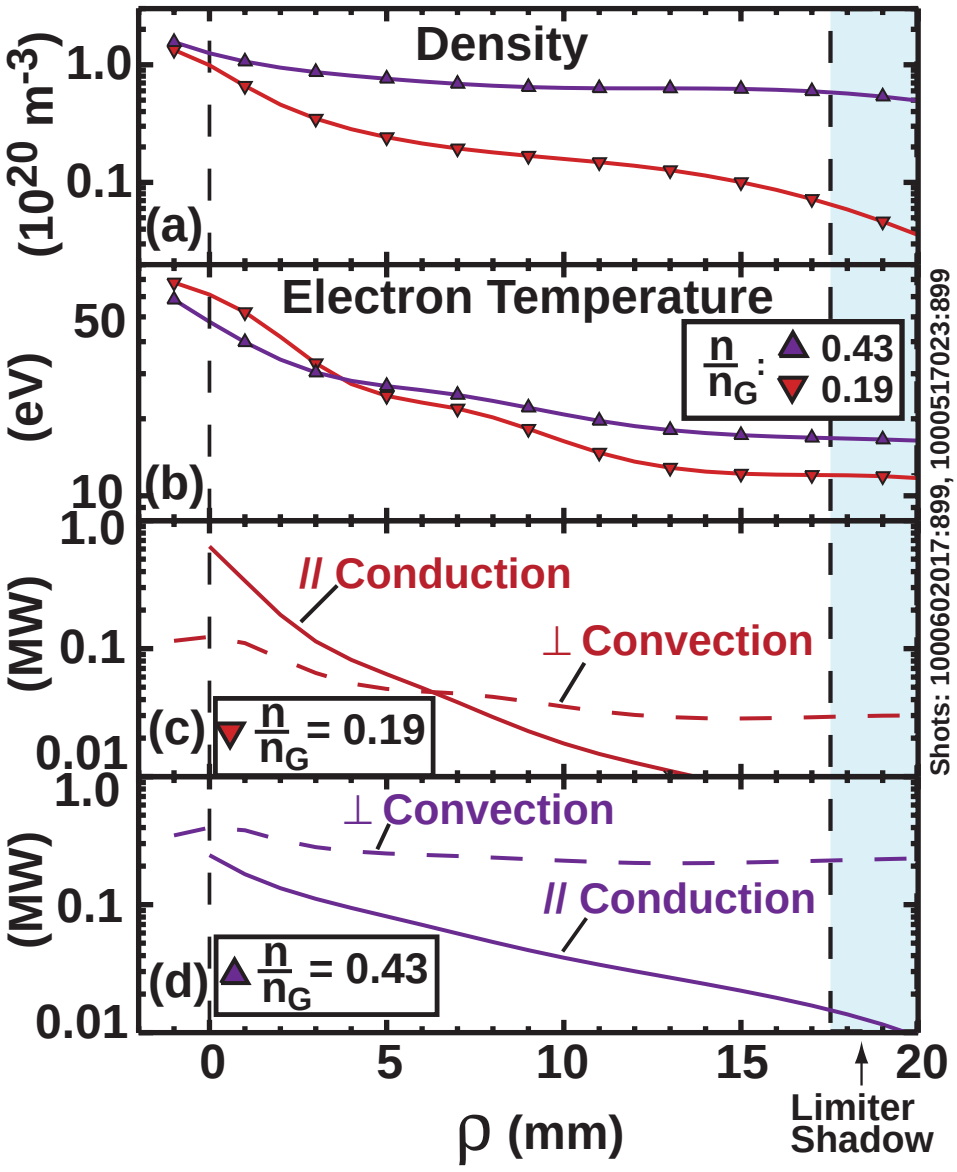

Fig. 5. Cross-field profiles from two discharges: (a) density and (b) electron temperature (both spline fits to probe data) at low (▼) and moderate line-average density (▲), (c) cross-field heat convection (Q_{conv}) and cross-field heat flux (Q_{div}) necessary to support parallel conduction losses to the divertor for the low density discharge, and (d) Q_{conv} and Q_{div} for the moderate density discharge.

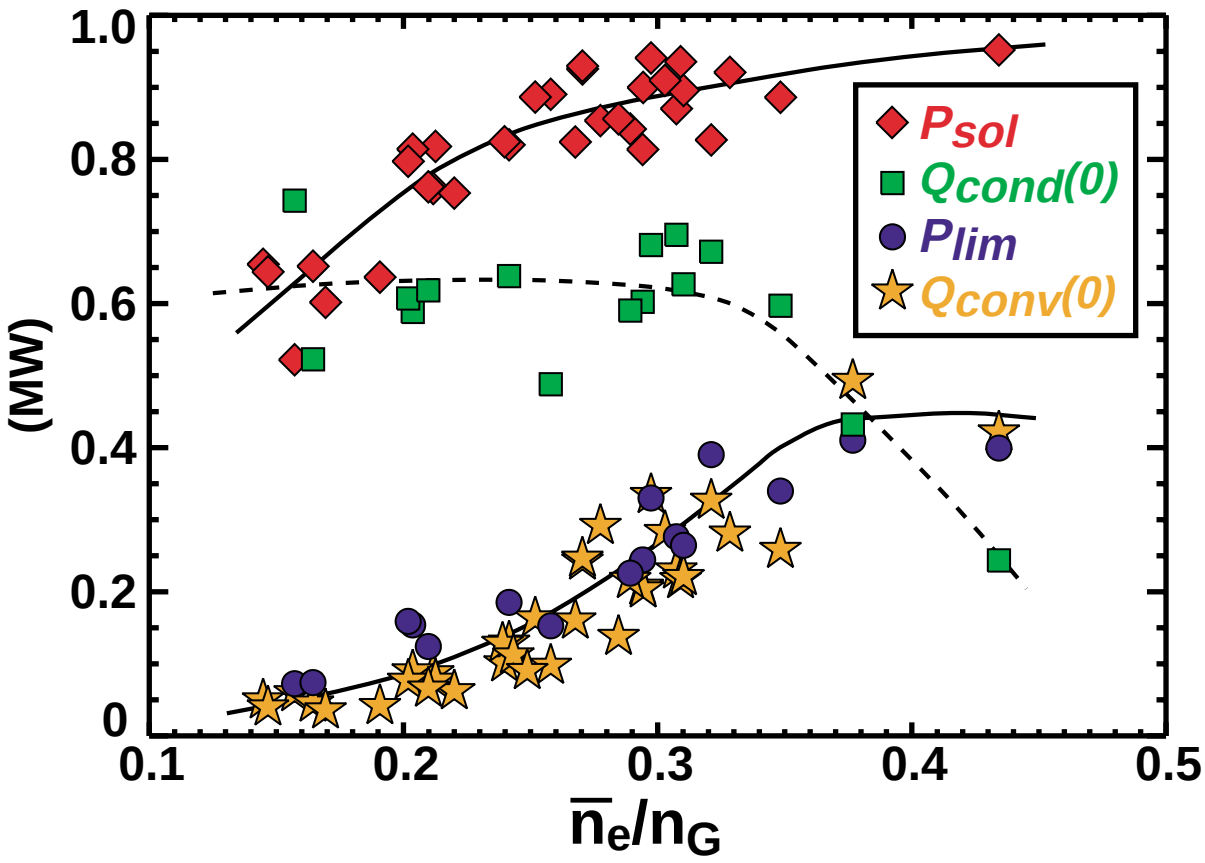

Fig. 6. Cross-check of heat flux estimates: (◆) power flowing into SOL based on input power minus core radiation, (■) power conducted along field lines to divertor based on $T_e^{7/2}$ integration across SOL, (●) power convected across a flux surface 4 to 5 mm beyond the shadow of main-chamber limiters based on $5\ T_e$ times the limiter-shadow particle flux probe measurement shown in Fig.2, and (★) power convected across separatrix based on $A_{LCFS}\ 5\ T_e\ \Gamma_\perp$, where $\Gamma_\perp$ is estimated from local particle balance model (section III.B). Horizontal axis is line-averaged discharge density normalized to Greenwald density.

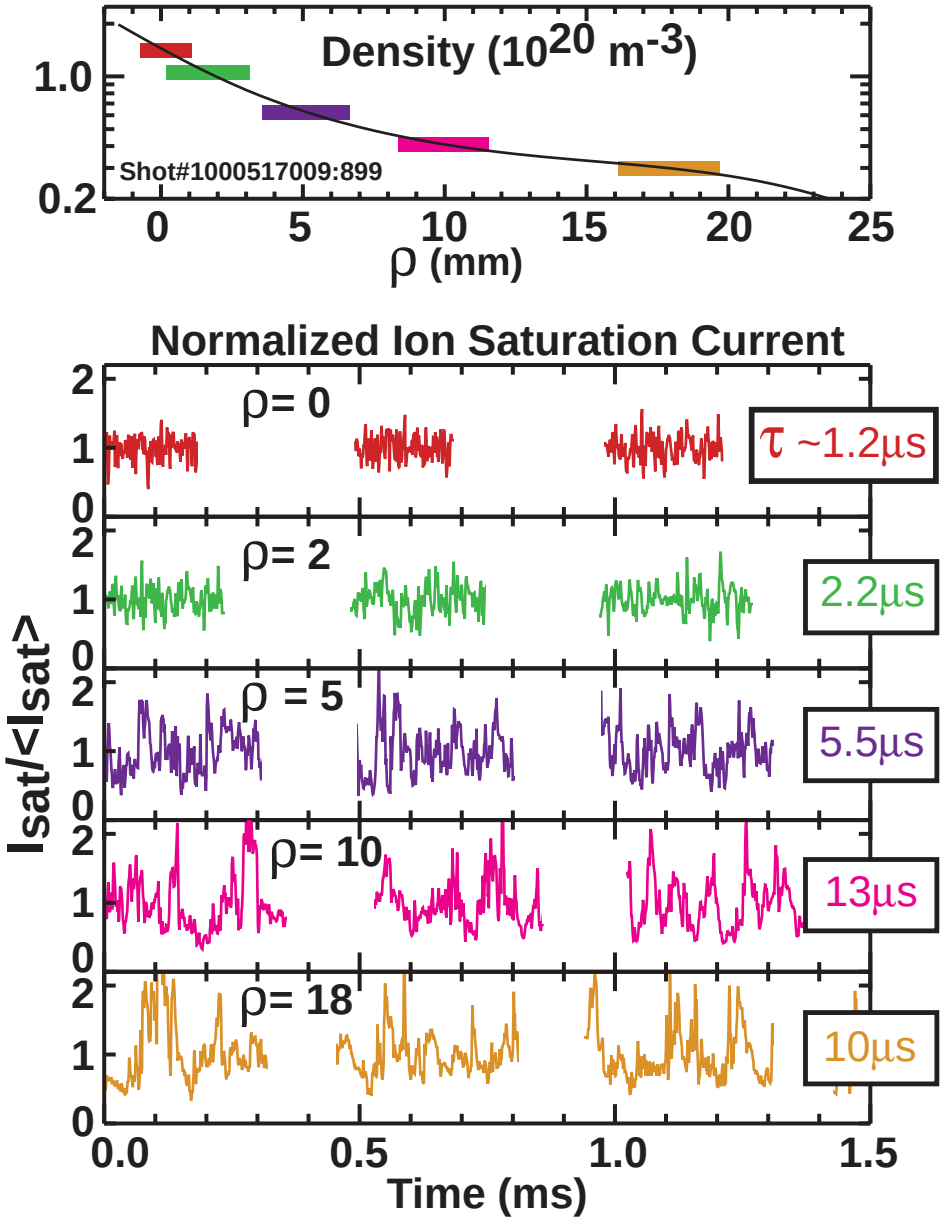

Fig. 7. Top panel: Cross-field density profile from horizontal scanning probe (spline fit). Bottom panels: time snapshots of $I_{sat}/\langle I_{sat}\rangle$ at different locations (indicated by ρ value) as the probe traverses the SOL plasma. The breaks in the time series correspond to times when the probe is not biased in ion saturation. Note: The time axis is relative; Each snapshot is acquired at a different time over the probe s trajectory. Digital sampling rate is 1 MHz. Characteristic e-folding times (τ) of the auto-correlation function for the time series are indicated.

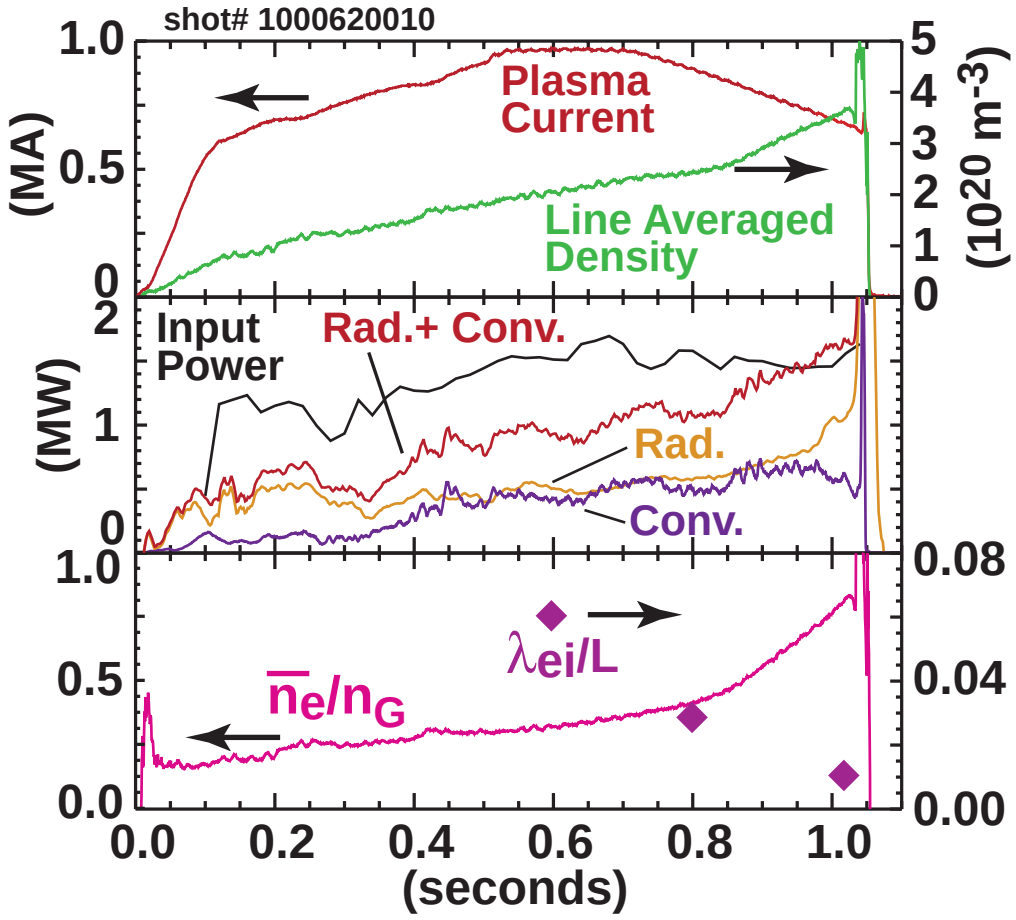

Fig. 8. Time evolution of a discharge used to study SOL transport and fluctuation behavior near the density limit. Top panel: plasma current and line-averaged density ($\bar{n}_e$). Middle panel: input power, total radiated power, and an estimate of heat convection onto main-chamber limiter surfaces based on limiter-shadow particle flux probe. Lower panel: $\bar{n}_e$ normalized to Greenwald density (n_G) and electron-ion mean free path normalized to 1/2 the magnetic connection length (λ_{ei}/L) at ρ = 1 mm obtained from the three times when the horizontal scanning probe is operated.

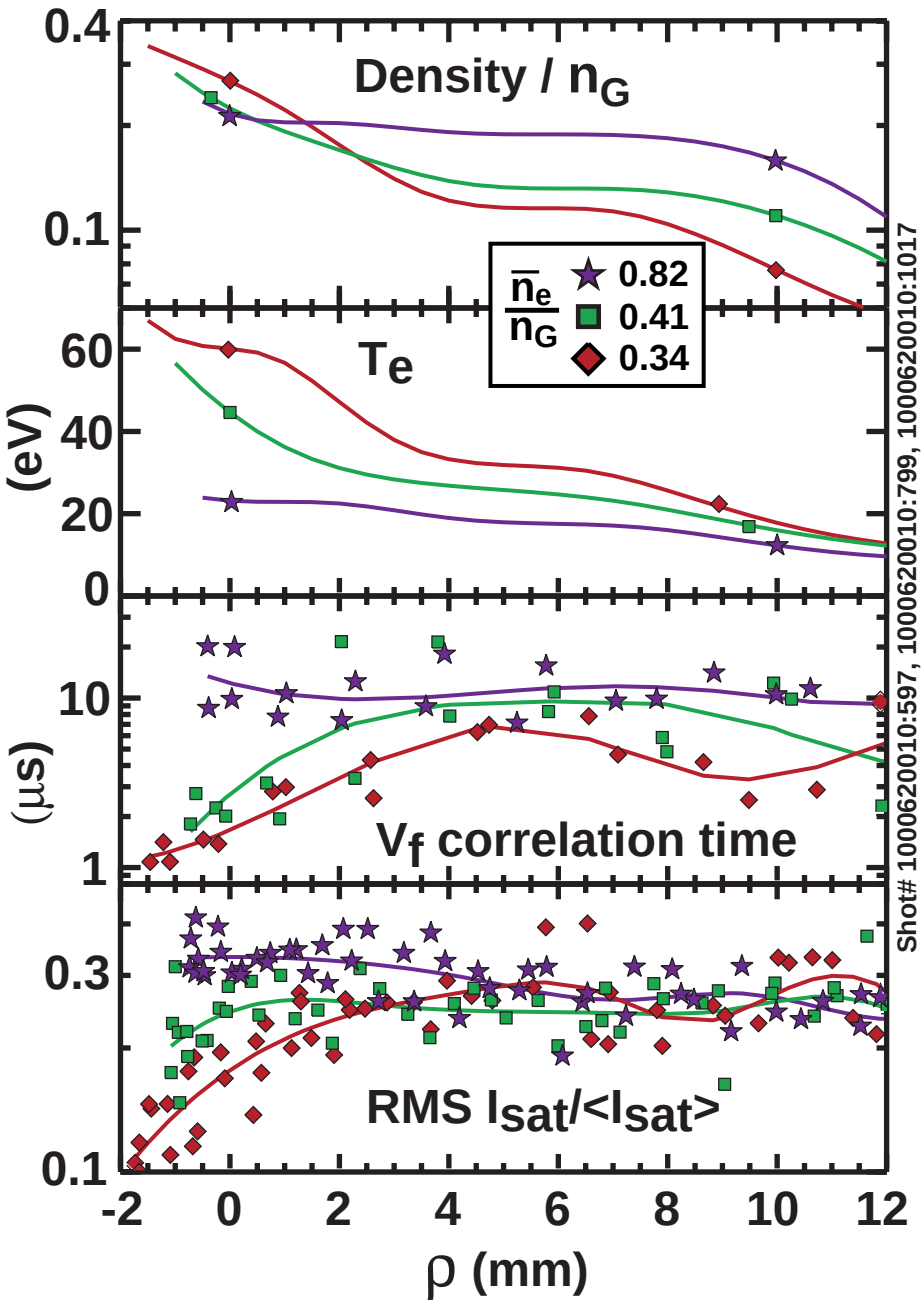

Fig. 9. SOL profiles at three times in the discharge shown in Fig.8. Top two panels: density (normalized to Greenwald density) and electron temperature profiles (spline fits to probe data). Third panel: profiles of characteristic auto-correlation times (τ) inferred from floating potential fluctuations over 2 msec time intervals. Bottom panel: profiles of RMS fluctuation level of ion saturation current normalized by the mean value over 0.2 to 0.3 msec time intervals. In the bottom two panels, data points and corresponding spline fits are shown.